

A procedure for the preparation of Ti-Beta zeolites for catalytic epoxidation with hydrogen peroxide†

Cite this: *Green Chem.*, 2014, **16**, 2281

Bo Tang,^a Weili Dai,^a Xiaoming Sun,^{a,b} Naijia Guan,^a Landong Li^{*a} and Michael Hunger^b

Ti-Beta zeolite has been successfully prepared *via* a reproducible and scalable two-step post-synthesis strategy, which consists of creating vacant T sites with associated silanol groups by dealumination of H-Beta and subsequent dry impregnation of the resulting Si-Beta with titanocene dichloride. The mechanism of Ti incorporation into the framework of Beta is investigated by diffuse reflectance infrared Fourier transform (DRIFT) and multinuclear solid-state nuclear magnetic resonance (SSNMR) spectroscopy. Characterization results obtained from diffuse reflectance ultraviolet-visible (UV-vis) and X-ray photoelectron spectroscopy (XPS) reveal that the majority of incorporated Ti species exist in the form of isolated tetrahedrally coordinated Ti(IV) in the zeolite framework while a minority exists in the form of isolated octahedrally coordinated Ti(VI) at framework or extra-framework positions. The obtained Ti-Beta zeolites are highly active and selective catalysts for the epoxidation of unsaturated ketones, *e.g.* 2-cyclohexen-1-one, with hydrogen peroxide as an oxidant. A quasilinear correlation between the epoxidation rate and the number of framework Ti(IV) species could be drawn evidencing that these Ti(IV) species are responsible for the epoxidation activity of the Ti-Beta zeolites under study. The impact of preparation parameters and reaction conditions on the catalytic performances of the Ti-Beta zeolites in the epoxidation of unsaturated organic compounds with hydrogen peroxide is discussed in detail.

Received 12th December 2013,
Accepted 18th January 2014

DOI: 10.1039/c3gc42534g

www.rsc.org/greenchem

1. Introduction

Incorporation of metals into zeolites brings about many interesting properties, which can be utilized for heterogeneous catalysis. Of particular importance is the exploitation of TS-1, being a Ti(IV)-containing MFI-type zeolite, as a robust catalyst in green oxidation reactions with hydrogen peroxide, such as hydroxylation of aromatics, oxidation of alcohols to carboxyl compounds, epoxidation of propylene, and cyclohexanone ammoxidation.^{1–4} The success of TS-1 as a milestone has initiated extensive research on sustainable oxidation reactions catalyzed by Ti(IV)-containing zeolites. On the other hand, the catalytic application of TS-1 is limited to relatively small substrate molecules due to its 10-ring pore system (MFI: [100] 0.51 × 0.55 nm ↔ [010] 0.53 × 0.56 nm), and therefore, Ti(IV)-containing zeolites with larger pore sizes are required to overcome the diffusion restrictions for reactant molecules.^{5–8} A

promising way is by the Ti(IV)-modification of Beta zeolites characterized by 12-ring pores (BEA: ⟨100⟩ 0.66 × 0.67 nm ↔ [001] 0.56 × 0.56 nm), which substantially expands the substrate scope for liquid-phase oxidation on Ti(IV)-containing zeolites.⁹ Up to now, Ti-Beta zeolites have been successfully applied in the epoxidation of linear and cyclic olefins, monoterpenes, methyl esters of fatty acids, unsaturated alcohols, and α,β-unsaturated carbonyls with hydrogen peroxide (Scheme 1). In all these reactions, Ti-Beta zeolites act as active heterogeneous catalysts with high hydrogen peroxide efficiency.¹⁰

The preparation of Ti-Beta is an essential issue to be addressed. Generally, Ti can be directly incorporated into the Beta zeolites during the formation of the BEA framework, and different procedures, *e.g.* conventional hydrothermal crystallization,⁹ dry-gel conversion,¹¹ and crystallization in fluoride medium,¹² have been reported. Although highly active Ti-Beta zeolites can be obtained *via* direct synthesis routes, most of these routes are quite complicated and time-consuming. Accordingly, a lack of reproducibility in the direct synthesis procedure of Ti-Beta zeolites may be complained and large-scale synthesis for industrial applications is yet to be accomplished. In this context, alternative post-synthesis strategies have been developed for the preparation of Ti-Beta zeolites. Chemical vapor deposition (CVD) offers the possibility of

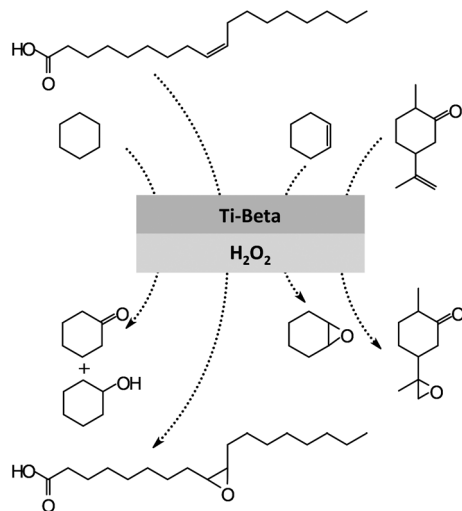
^aKey Laboratory of Advanced Energy Materials Chemistry (Ministry of Education), College of Chemistry, Nankai University, Tianjin 300071, P. R. China.

E-mail: lild@nankai.edu.cn; Fax: (+)86 22 23500341; Tel: (+)86 22 23500341

^bInstitute of Chemical Technology, University of Stuttgart, 70550 Stuttgart, Germany.

E-mail: michael.hunger@itc.uni-stuttgart.de

†Electronic supplementary information (ESI) available. See DOI: 10.1039/c3gc42534g



Scheme 1 Examples of chemical transformations realized by Ti(IV)-containing Beta zeolites and hydrogen peroxide.

preparing Ti(IV)-containing zeolites with titanium tetrachloride used as the titanium source deposited on the zeolite host.^{13,14} In addition, post-synthesis grafting of the organometallic precursor titanocene dichloride (Cp_2TiCl_2) on zeolite hosts has been reported for obtaining so-called single-site zeolite catalysts with a remarkable activity in the epoxidation of olefins.^{15–18} In comparison with titanium tetrachloride, Cp_2TiCl_2 seems to be a more suitable Ti source for the preparation of Ti(IV)-containing zeolites, because the latter is less reactive, less moisture-sensitive, and easier to handle. However, large amounts of hazardous chlorinated solvents are employed during the organometallic grafting process, which may also show negative effects on the incorporation of Ti into zeolite frameworks, resulting in poor reproducibility. Moreover, the ligand removal process may lead to the transformation of Ti species and the formation of unreactive bulk TiO_2 .

In a comprehensive consideration, a dry impregnation of zeolite Beta containing numerous defect SiOH groups with a Ti source, such as by carefully grinding a dealuminated zeolite Beta with a solid organometallic complex and performing a subsequent calcination of this physical mixture, is regarded as an ideal route for incorporating metal ions into the zeolite framework. In this procedure, no hazardous solvents are used and the absence of solvents completely prevents the solvation shell surrounding the Ti atoms, which could potentially lead to significant diffusion limitations inside the zeolite pores. Therefore, we focused on the development of a simple and scalable two-step post-synthesis procedure for preparing Ti-Beta zeolites based on the dry impregnation of dealuminated zeolite Beta with Cp_2TiCl_2 as a Ti source. Briefly, vacant T (T = Al) sites with associated silanol groups are first created by treating commercial H-Beta zeolite with concentrated nitric acid solution and the resulting Si-Beta zeolite is subsequently ground with the Ti precursor Cp_2TiCl_2 to produce a physical Si-Beta- Cp_2TiCl_2 mixture, followed by calcination to derive a Ti(IV)-containing zeolite Beta. This route is suitable for the

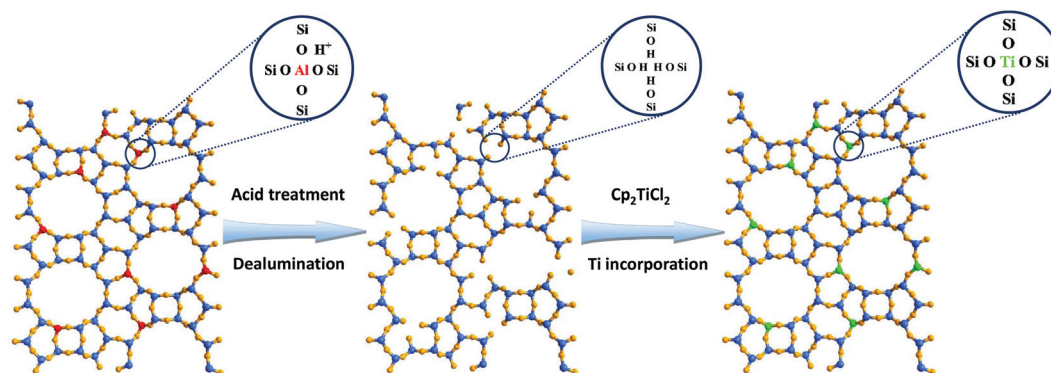
industrial production of Ti-Beta zeolites and it can be extended to the incorporation of other metal ions into a zeolite matrix providing that a dealumination of the zeolite host is possible and the organometallic precursor is available. These post-synthesis modified Ti-Beta zeolites are expected to be suitable catalysts for epoxidation reactions, one of the most important classes of organic transformations in fine chemical and pharmacy industries.^{19–22} Typically, the epoxidation of 2-cyclohexen-1-one, a type of cyclic unsaturated ketone, is selected as a model reaction to evaluate the catalytic performances of Ti-Beta zeolites using hydrogen peroxide as an oxidant in the present study. Furthermore, special emphasis has been laid on the mechanism of Ti incorporation into the framework of zeolite Beta and its effects on epoxidation activity.

2. Experimental

2.1. Sample preparation

Ti(IV)-containing zeolite Beta, *i.e.* Ti-Beta, was prepared *via* a two-step post-synthesis procedure consisting of the dealumination of a zeolite H-Beta to get a Si-Beta material and subsequent incorporation of Ti into the Si-Beta framework, as described in Scheme 2. To obtain a highly siliceous Si-Beta material ($n_{\text{Si}}/n_{\text{Al}} > 1800$), commercial H-Beta zeolite ($n_{\text{Si}}/n_{\text{Al}} = 13.5$, Sinopec Co.) was treated with 13 mol L^{-1} HNO_3 solution (20 mL g^{-1} zeolite) for 20 h and then washed with deionized water until the pH value of the filtrate was neutral. After drying at 353 K overnight, the Si-Beta powder was ground with an appropriate amount of Cp_2TiCl_2 rapidly to obtain an intimate mixture of the two solids. The Si-Beta- Cp_2TiCl_2 mixture was then calcined in flowing air at 823 K for 12 h to derive zeolite Ti-Beta. The obtained samples are assigned $n \text{ wt\%}$ Ti-Beta with weight percent (n) of Ti atoms on the dehydrated Si-Beta zeolite. In this study, four different Ti-Beta zeolites with Ti loadings of 1 wt%, 2 wt%, 3 wt%, and 5 wt% were prepared.

For comparison, a microporous TS-1 zeolite and a mesoporous Ti-grafted MCM-41 (denoted Ti-MCM-41) material were prepared according to the literature.^{15,23} In a typical synthesis of TS-1, tetraethyl orthotitanate was added dropwise to tetraethyl orthosilicate and the mixture was stirred for 2 h to obtain a clear solution, to which tetrapropylammonium hydroxide (TPAOH) and deionized water were added under stirring at room temperature and then heated to 353 K for 5 h to aid hydrolysis. The resulting gel mixture ($0.022\text{TiO}_2 : 1.0\text{SiO}_2 : 0.35\text{TPAOH} : 35\text{H}_2\text{O}$) was transferred into a Teflon-lined stainless steel autoclave for static crystallization at 448 K for 48 h. The solid products were recovered by centrifuging, washed with deionized water, dried at 353 K overnight and calcined in air at 823 K for 12 h. For the synthesis of Ti-MCM-41, siliceous MCM-41 (0.4 g)²⁴ was stirred with Cp_2TiCl_2 (0.02 g) in chloroform (10 mL) for 0.5 h. Then, triethylamine (1 mL) was added under stirring and the colour of the mixture gradually changed from red to yellow within 2 h, indicating the substitution of the chloride ligands by siloxide ligands. The yellow solid was



Scheme 2 Schematic representation of the incorporation of tetrahedrally coordinated Ti(IV) species into Beta zeolite.

separated by centrifuging and washed with chloroform three times, followed by calcination at 823 K for 12 h.

Ti(IV)-containing Beta zeolites with a designed Ti loading of 5.0 wt% (5 wt% Ti-Beta) were also prepared *via* different routes to investigate the influence of the preparation procedure on the catalytic properties of the various Ti-Beta zeolites. Briefly, zeolite TiO₂/Si-Beta-w was synthesized *via* wet impregnation, in which the Si-Beta support was suspended in cyclohexane and tetrabutyl orthotitanate (TBOT) was added. The mixture was refluxed at 341 K for 24 h and the solid was calcined in air at 823 K for 12 h to obtain the final product. Zeolite TiO₂/Si-Beta-m was prepared by mechanically mixing the Si-Beta support with TiO₂ (Degussa P25), followed by calcination at 823 K for 12 h to obtain the final product. Finally, zeolite Ti-H-Beta was prepared using the same procedure as that for the post-synthesis modified zeolite Ti-Beta except that H-Beta zeolite was used as the zeolite host instead of siliceous Si-Beta.

2.2. Sample characterization

X-ray diffraction (XRD) patterns of the sample materials were recorded on a Bruker D8 diffractometer with CuK α radiation ($\lambda = 1.54184 \text{ \AA}$) from 5° to 40° with a scan speed of $2\theta = 6.0^\circ \text{ min}^{-1}$.

Scanning electron microscopy (SEM) images were obtained using a Hitachi S-4800 microscope.

The chemical compositions of the samples under study were determined by inductively coupled plasma emission spectrometry (ICP-AES) on a Thermo IRIS Intrepid II XSP atomic emission spectrometer.

The surface areas and pore volumes of the calcined samples were measured by means of nitrogen adsorption at 77 K on a Quantachrome iQ-MP gas adsorption analyzer. Before the nitrogen adsorption, samples were dehydrated at 473 K for 2 h. The total surface area was calculated *via* the Brunauer Emmett Teller (BET) equation and the microporous pore volume was determined using the *t*-plot method.

Diffuse reflectance ultraviolet-visible (UV-vis) spectra were recorded in the region of 200–700 nm under air conditions and against BaSO₄ using a Varian Cary 300 UV-vis spectrophotometer.

Raman analysis was carried out using a Renishaw InVia Raman spectrometer and the spectra were obtained with the green line of an argon-ion laser (514.53 nm) in a micro-Raman configuration.

X-ray photoelectron spectra (XPS) were recorded on a Kratos Axis Ultra DLD spectrometer with a monochromated Al-K α X-ray source ($h\nu = 1486.6 \text{ eV}$), hybrid (magnetic/electrostatic) optics and a multi-channel plate and delay line detector (DLD). All spectra were recorded by using an aperture slot of 300×700 microns. Survey spectra were recorded with a pass energy of 160 eV and high-resolution spectra with a pass energy of 40 eV. Accurate binding energies ($\pm 0.1 \text{ eV}$) were determined with respect to the position of the adventitious C 1s peak at 284.8 eV.

Diffuse reflectance infrared Fourier transform (DRIFT) spectra of samples were measured on a Bruker Tensor 27 spectrometer with 128 scans at a resolution of 2 cm^{-1} . Self-supporting pellets made of sample material were placed in the reaction chamber and pretreated in flowing dry air at 473 K for 1 h. The spectra were recorded in dry air against KBr as the background.

Solid-state nuclear magnetic resonance (NMR) experiments were performed on a Bruker Avance III 400WB spectrometer at resonance frequencies of 400.1, 104.3, and 79.5 MHz for ¹H, ²⁷Al, and ²⁹Si, respectively. The experimental conditions are as follows: single pulse excitation of $\pi/2$ for ¹H, $\pi/6$ for ²⁷Al, and $\pi/4$ for ²⁹Si, with repetition times of 20 s for ¹H and ²⁹Si, and 0.5 s for ²⁷Al MAS NMR spectroscopy. The ¹H and ²⁷Al MAS NMR spectra were recorded with a sample spinning rate of 8 kHz, while the ²⁹Si MAS NMR spectra were obtained with 4 kHz. ¹H NMR MAS NMR measurements were performed using dehydrated samples, which were dehydrated at 673 K at a pressure below 10^{-2} Pa for 12 h. ²⁷Al and ²⁹Si MAS NMR measurements were performed using hydrated samples. For this purpose, the dehydrated sample materials were exposed to the vapor over a saturated aqueous Ca(NO₃)₂ solution at ambient temperature for at least 12 h.

2.3. Catalytic evaluation

The catalytic epoxidation reactions were performed in a 25 mL round-bottom glass flask equipped with a cryogenic-liquid

condenser under atmospheric pressure. Typically, 5 mmol of 2-cyclohexen-1-one or its derivatives, 0.1 g of catalyst, and 10 mL of acetonitrile (or other solvents) were added to the vessel and mixed vigorously by a magnetic stirrer. The vessel was heated to the desired reaction temperature and then 7.5 mmol of H₂O₂ (31 wt% aqueous solution) were added into the vessel under stirring. After the reaction, liquid-phase products were qualitatively analyzed by a Shimadzu GC-MS QP2010 SE and quantitatively determined by a Shimadzu 2010 GC equipped with an Agilent HP-5MS column (30 m × 0.25 mm × 0.25 μm), while chlorobenzene was used as an internal standard. Carbon balance of over 95% was obtained for all experiments. The conversion of the substrate and the selectivity of the products were calculated as follows:

$$\text{Substrate conversion (mol\%)} = \frac{(\text{initial moles} - \text{final moles})}{\text{initial moles}} \times 100\%$$

$$\text{Product selectivity (\%)} = \frac{\text{moles of the product}}{\text{moles of all product}} \times 100\%$$

Recycling tests of Ti-Beta zeolites were performed as follows. After the reaction at 343 K in acetonitrile for 5 h, the catalyst samples were recovered by centrifugation and washed with acetonitrile. After repeating this procedure three times, the Ti-Beta samples were dried at 353 K overnight and calcined in static air at 823 K for 6 h.

3. Results and discussion

3.1. Evidences for Ti incorporation into the zeolite framework

Possible structure changes of the Beta zeolites due to the post-synthesis procedures were investigated by X-ray diffraction and the corresponding powder patterns are shown in Fig. 1. Typical diffraction lines characteristic for the BEA topology are observed for H-Beta, Si-Beta, and Ti-Beta, indicating that the framework structure is well preserved after dealumination and Ti incorporation. For 5 wt% Ti-Beta, no obvious diffraction lines corresponding to titanium species can be observed, probably due to the high dispersion of Ti species. The well preserved microporous BEA structure after dealumination and Ti incorporation is further confirmed by the nitrogen physisorption (Fig. S1†), in which similar and typical type I adsorption/desorption isotherms can be observed for all samples.

The physicochemical properties of H-Beta, Si-Beta, and 1 to 5 wt% Ti-Beta are summarized in Table 1. All samples exhibit similar BET surface areas (567–620 m² g⁻¹) and micropore volumes (0.196–0.204 cm³ g⁻¹), confirming that the textural properties of the Beta zeolite are well preserved after dealumination and Ti incorporation. ICP analysis results reveal that the *n*_{Si}/*n*_{Al} ratio of the parent H-Beta sharply increases from 13.5 to over 1800 for the dealuminated Si-Beta, indicating that the latter is essentially free of Al. Theoretically, the maximal Ti

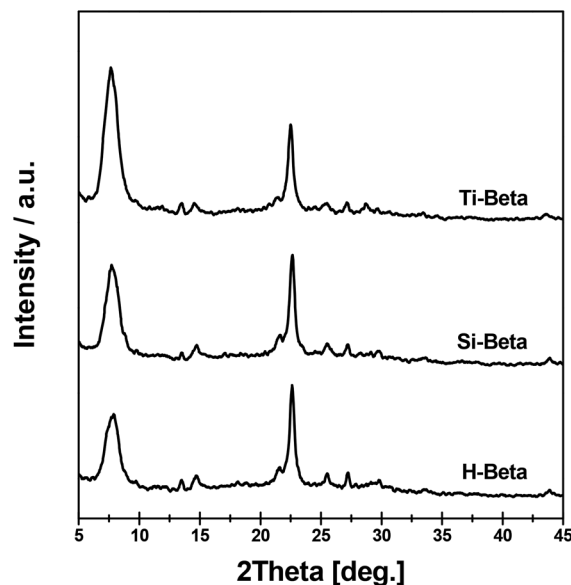


Fig. 1 XRD patterns of H-Beta, Si-Beta, and 5 wt% Ti-Beta.

Table 1 Physicochemical properties of H-Beta, Si-Beta, and Ti-Beta zeolites

Sample	<i>n</i> _{Si} / <i>n</i> _{Al} ^a	Ti loading ^a (wt%)	Surface area ^b (m ² g ⁻¹)	Pore volume ^c (cm ³ g ⁻¹)
H-Beta	13.5	/	590	0.204
Si-Beta	>1800	/	620	0.210
1 wt% Ti-Beta	>1800	1.0	610	0.203
2 wt% Ti-Beta	>1800	1.9	598	0.200
3 wt% Ti-Beta	>1800	2.8	581	0.198
5 wt% Ti-Beta	>1800	4.1	567	0.196

^a Determined by ICP. ^b Specific surface area obtained by the BET method. ^c Calculated from *t*-plot.

loading is calculated to be 4.9 wt% assuming that one Ti atom replaces one framework Al atom. At relatively low Ti loadings (1 wt%, 2 wt%, 3 wt%), the actual Ti loading analyzed by ICP is very close to the desired value. While at the highest Ti loading of 5 wt%, the actual Ti loading is distinctly lower (4.1 wt%), hinting at approaching of saturation of the Ti incorporation and a loss of Ti during the calcination process. The existence of residual chloride and carbon could be excluded by XPS and element analysis, respectively.

The SEM images of the H-Beta, Si-Beta, and 5 wt% Ti-Beta are shown in Fig. S2.† Obviously, a similar morphology can be observed for the three samples, ruling out the possibility of morphology changes after dealumination and Ti incorporation. The crystal particles of 5 wt% Ti-Beta are observed to be uniform nanoparticles with a size of 50–80 nm. Such small crystal particles are presumed to encounter less diffusion limitation in converting bulky substrate molecules.

Fig. S3† shows the FTIR spectra in the framework vibration region (700–1400 cm⁻¹) of Si-Beta and 2 to 5 wt% Ti-Beta samples. The vibrational band at 948 cm⁻¹ observed for Si-Beta is probably due to the presence of a large amount of

defect sites, originating from extracting framework Al atoms during the dealumination process, as confirmed by the SiOH bands in the hydroxyl stretching region of the DRIFT spectra (*vide infra*, section 3.2). After the introduction of Cp_2TiCl_2 and subsequent calcination, the 948 cm^{-1} band disappears, indicating the binding of Ti atoms at the former defect sites (as illustrated in Scheme 2, the Ti incorporation mechanism will be further discussed in the following section). Meanwhile, a new FTIR band centered at 962 cm^{-1} appears for Ti-Beta samples, which is characteristic of titanosilicates as suggested by earlier reports.^{7,25,26} This can be seen as an evidence of the successful incorporation of Ti species into the zeolite framework.

To understand the coordination of the incorporated Ti species in the microporous structure, UV-vis analysis was performed with calcined Ti-Beta zeolites and the corresponding spectra are shown in Fig. 2. Ti-Beta samples with different Ti loadings essentially exhibit an intense band centered at 45900 cm^{-1} (218 nm) arising from oxygen to Ti(IV) ligand to metal charge transfer (LMCT).^{11,14,27} In addition, a shoulder band centered at 38700 cm^{-1} (258 nm), corresponding to octahedral Ti(VI) in framework or extra-framework positions,^{16,28} can be observed especially at relatively high Ti loadings (3.0 and 5.0 wt%). The band centered at 45900 cm^{-1} increases in intensity with increasing Ti loading, indicating that Ti species are mainly incorporated into the framework of Beta. For Ti-Beta zeolites with different Ti loadings, no band centered at below 30300 cm^{-1} ($>330\text{ nm}$) occurred and the existence of bulk anatase TiO_2 can be excluded. This is further confirmed by Raman analysis. As shown in Fig. S4,[†] no Raman active modes corresponding to anatase TiO_2 can be observed in post-synthesized Ti-Beta even at the highest Ti loading of 5 wt%.

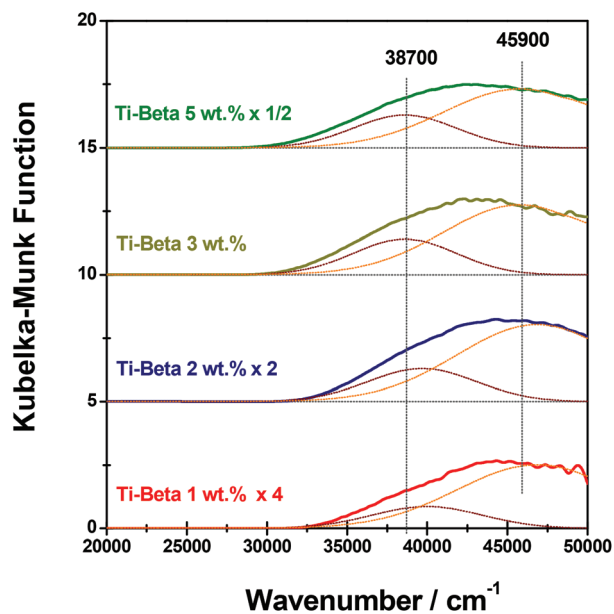


Fig. 2 UV-vis spectra of calcined Ti-Beta zeolites with different Ti loadings of 1 to 5 wt%.

The existing states of Ti species in as-synthesized Ti-Beta were further investigated by XPS and the results are shown in Fig. 3. In the Ti 2p region, signals at binding energies of 458.4, 459.3, 464.1, and 465.2 eV appeared for all samples. Generally, the binding energy values of 458.4 and 464.1 eV are assigned to $2p_{3/2}$ and $2p_{1/2}$ photoelectrons of tetrahedrally coordinated framework Ti(IV) species.^{29,30} Binding energy values of 459.3 and 465.2 eV, on the other hand, hint to $2p_{3/2}$ and $2p_{1/2}$ photoelectrons of octahedrally coordinated Ti(VI) species, either in framework or at extra-framework positions.^{29–31} It is quite clear that tetrahedrally coordinated framework Ti(IV) atoms are the dominating species (85–95%) in the Ti-Beta samples, consistent with the results of UV-vis spectroscopy. On the other hand, a significant increase in the percentage of Ti(VI) species from 5 to 15% was observed with increasing Ti loadings from 1 to 5 wt%.

Based on the characterization results from XRD, nitrogen physisorption and SEM, the framework structure of Beta zeolites is well preserved after dealumination and Ti incorporation. According to the results of UV-vis spectroscopy and XPS analysis, the majority of Ti species are successfully incorporated into the BEA framework. Since all samples have been calcined at 823 K for 12 h, the calcined Ti-Beta samples are expected to be stable materials for applications in heterogeneous catalysis.

3.2. Mechanism of Ti incorporation into the zeolite framework

According to the above-mentioned characterization results, we propose that mainly tetrahedrally coordinated Ti species are incorporated into the Beta zeolite framework by interacting with SiOH groups at defect sites formed upon dealumination.

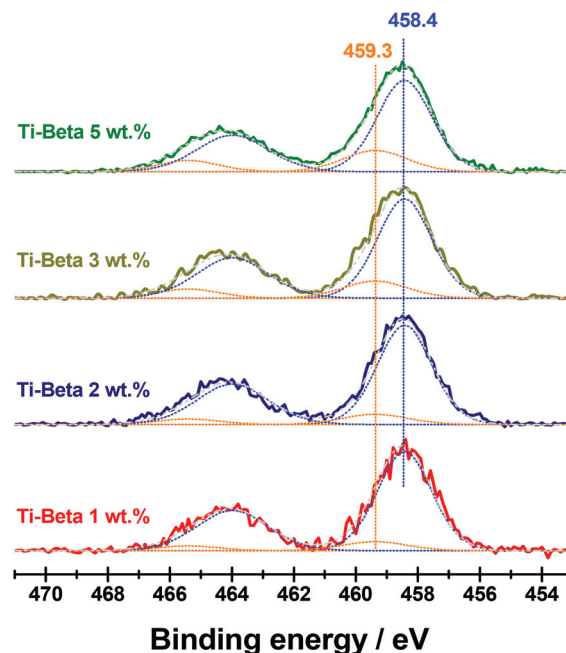


Fig. 3 Ti 2p XPS of Ti-Beta with different Ti loadings.

In order to confirm this assumption, the mechanism of the Ti incorporation into the zeolite framework is further investigated by means of DRIFT and NMR spectroscopy.

Fig. 4 displays the hydroxyl stretching region of the DRIFT spectra of calcined H-Beta, Si-Beta, and 5 wt% Ti-Beta. The parent H-Beta exhibits two major bands at 3740 and 3600 cm^{-1} , corresponding to isolated terminal silanol (SiOH) and bridging hydroxyl groups (Si(OH)Al), respectively.^{14,32} Two bands at 3775 and 3655 cm^{-1} associated with Al–OH groups of extra-framework aluminum species and a broad weak band at 3540 cm^{-1} corresponding to hydrogen-bonded Si–OH groups can also be observed.^{32,33} After dealumination with concentrated HNO_3 solution, the 3775, 3655, and 3600 cm^{-1} bands related to Al species could not be detected any more due to complete removal of the Al atoms from the zeolite framework, which is consistent with the ICP analysis ($n_{\text{Si}}/n_{\text{Al}} > 1800$). Simultaneously, an increase in the intensity of the SiOH band at 3745 cm^{-1} and the appearance of a new, very broad band at around 3520 cm^{-1} are observed, indicating the formation of defect sites at the zeolite framework. Specifically, the band at around 3520 cm^{-1} indicates the formation of hydroxyl nests with hydrogen-bonded SiOH groups located at the vacant T sites of the dealuminated Si-Beta framework (Scheme 2, acid treatment step), which is in line with earlier assignments.^{32–35} The incorporation of Ti atoms into Si-Beta induces a small decrease in intensity of the band at 3740 cm^{-1} , indicating that Ti atoms bind to terminal oxygen atoms and replace silanol groups to some extent in the case of a high Ti loading (5 wt%). This may result in the formation of some extra-framework Ti species in Ti-Beta, often as octahedrally coordinated species, as revealed by UV-vis spectroscopy and XPS (Fig. 2 and 3). In contrast, the strong decrease of the 3520 cm^{-1} band, also

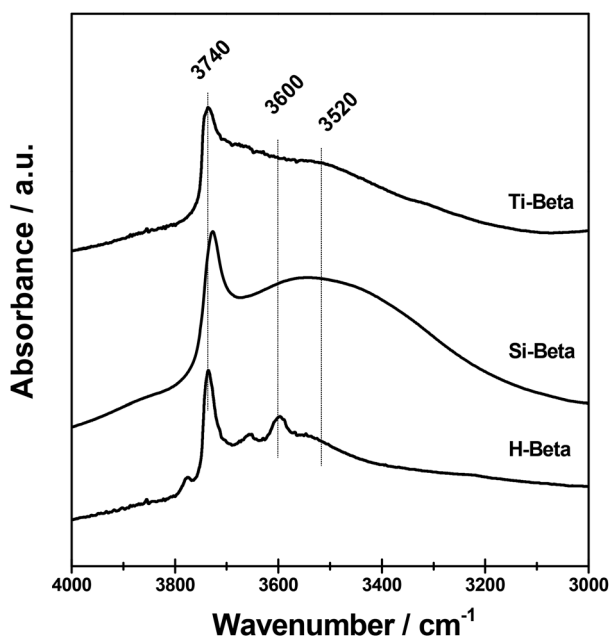


Fig. 4 DRIFT spectra in the hydroxyl stretching vibration region of H-Beta, Si-Beta, and Ti-Beta (5.0 wt%).

observed with increasing Ti loading, reveals the incorporation of Ti species mainly into the vacant T sites of the dealuminated zeolite framework.

The results of the solid-state NMR spectroscopic studies are shown in Fig. 5. The ^{27}Al MAS NMR spectra of H-Beta (left, bottom) consists of an intense signal at *ca.* 54 ppm ascribed to framework Al atoms in tetrahedral oxygen coordination and an additional weak signal at *ca.* 0 ppm due to extra-framework Al atoms in octahedral coordination.³⁶ Upon treating with concentrated HNO_3 solution, these two signals disappear completely, indicating that almost all of Al species in the Beta zeolite were removed by dealumination (left, top).

The ^{29}Si MAS NMR spectra of H-Beta show a series signals at –116, –113, –106, and –103 ppm (Fig. 5, middle). The signals at –116 and –113 ppm are attributed to framework $\text{Si}(\text{OSi})_4$ species (Q^4) at two different crystallographic sites,¹⁴ while the signal at –103 ppm is attributed to framework $\text{Si}(\text{OSi})_3(\text{OH})$ species (SiOH groups, Q^3) at defect sites,^{36,37} while the signal at –105 ppm is due to framework Si atoms with one Al neighbor, *i.e.* $\text{Si}(\text{OSi})_3(\text{OAl})$ species (Q^4).^{36–38} As a result of the dealumination, the intensities of signals due to Q^4 silicon species remain nearly unchanged, while the intensities of the signal due to SiOH groups (Q^3 species) decrease distinctly. Simultaneously, the signal caused by $\text{Si}(\text{OSi})_3(\text{OAl})$ species almost disappeared. These results clearly indicate the removal of framework Al atoms upon dealumination and the resulting changes of the SiOH defect sites in the Beta zeolite. The incorporation of Ti atoms into the Si-Beta framework does not cause obvious changes in the ^{29}Si MAS NMR spectra since the decrease of the Q^3 signal (SiOH) is compensated by the increase of the $\text{Si}(\text{OSi})_3(\text{OTi})$ signal.

In the ^1H MAS NMR spectrum of H-Beta (Fig. 5, right, bottom), a strong signal at 1.5 ppm and two weak signals at 2.5 and 3.9 ppm can be observed. These signals are due to silanol groups at framework defects (1.5 ppm), hydroxyl groups at extra-framework Al species (2.5 ppm), and bridging hydroxyl (Si(OH)Al) groups (3.9 ppm),^{39–41} respectively. The dealumination process leads to disappearance of hydroxyl groups associated with framework as well as extra-framework Al species responsible for the signals at 2.5 and 3.9 ppm, respectively. On the other hand, the intensity of the signal due to SiOH groups at framework defects (1.5 ppm) increases strongly and a new signal at 2.7 ppm emerges. Obviously, dealumination of H-Beta creates additional framework defects covered with SiOH groups. A reasonable explanation for the relatively high chemical shift of the silanol signal at 2.7 ppm is hydrogen bonds of some of these SiOH groups with neighboring framework oxygen species inside silanol nests. That is, vacant T sites in the zeolite framework are formed during the dealumination process and hydroxyl nests are formed, which agrees with the results of DRIFT spectroscopy (Fig. 4). The introduction of Ti into Si-Beta and subsequent calcination result in a dehydroxylation of the silanol groups at framework defects and hydroxyl nests, while exclusively the ^1H MAS NMR signal of non-interacting defect SiOH groups remains, which is slightly shifted to 1.9 ppm.

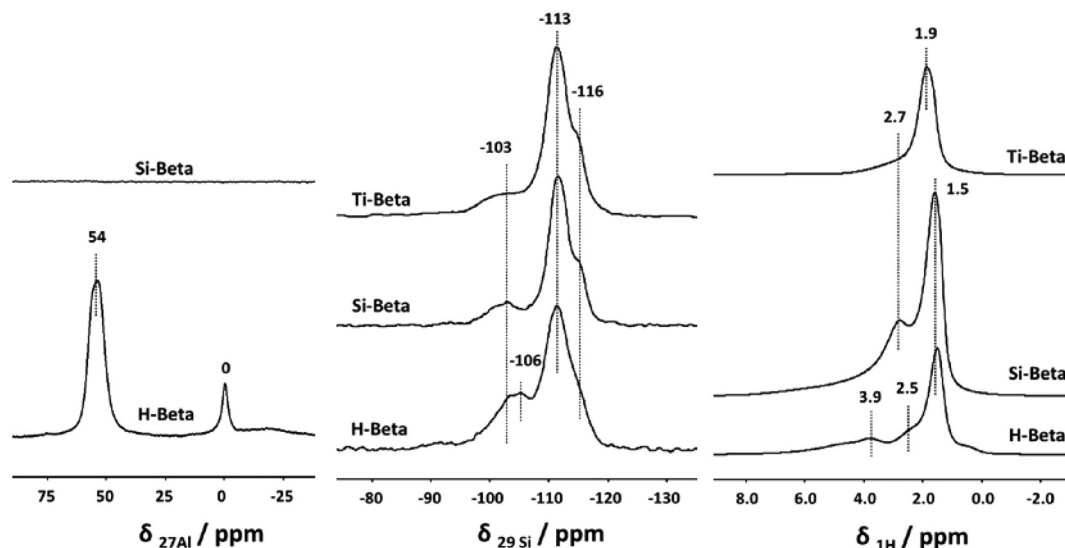


Fig. 5 ^{27}Al , ^{29}Si , and ^1H MAS NMR spectra of H-Beta, Si-Beta, and 5 wt% Ti-Beta.

Based on the results of DRIFT and solid-state NMR spectroscopy, the two-step mechanism of Ti incorporation into the zeolite Beta framework can be described as follows (Scheme 2): in the first step, the complete dealumination of zeolite H-Beta forms a large number of vacant T sites causing hydroxyl nests. In the second step, the organometallic Ti complex interacts with silanol nests and isolated defect SiOH groups of Si-Beta leading to replacement of their hydroxyl protons by Ti species, which causes Ti incorporation into the zeolite framework upon calcination.

3.3. Catalytic properties of Ti-Beta in epoxidation

3.3.1. Effects of structural features of Ti-zeolite. The catalytic activity of the post-synthesis modified Ti-Beta, together with the reference materials TS-1 and Ti-MCM-41, were investigated using the epoxidation of 2-cyclohexen-1-one as a model reaction. As shown in Fig. 6, the 2-cyclohexen-1-one conversion increases with time-on-stream for all Ti-zeolite catalysts with a similar Ti loading of *ca.* 2 wt%, while the selectivity to epoxide decreases. Obviously, Ti-Beta is much more active and selective than TS-1 and Ti-MCM-41. Typically, a turnover frequency (TOF) of 88.2 h^{-1} is obtained for Ti-Beta (calculated at time-on-stream of 0.5 h, assuming that all Ti species are catalytically active sites), more than four times higher than that of TS-1 (19.7 h^{-1}) and Ti-MCM-41 (17.6 h^{-1}).

The low activity of TS-1 may be due to steric limitations. Obviously, there is a strong diffusion hindrance for the reactant 2-cyclohexen-1-one with large kinetic diameter in the 10-ring pores of TS-1 (MFI: $[100] 0.51 \times 0.55\text{ nm} \leftrightarrow [010] 0.53 \times 0.56\text{ nm}$), so that the epoxidation reaction can only take place on the surface active sites near the pore openings and at a very small content of Ti sites acting as accessible catalytic sites. Ti-MCM-41 processes large mesopores of *ca.* 6 nm in diameter without diffusion limitations for the reactant 2-cyclohexen-1-one, and its low activity probably originates from an intrinsic

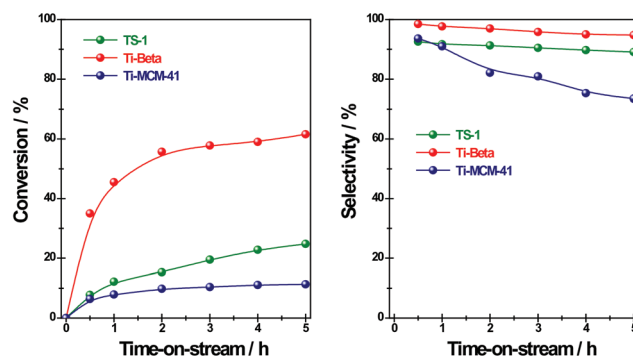


Fig. 6 Alkene conversion (left) and epoxide selectivity (right) in the 2-cyclohexen-1-one epoxidation on Ti-Beta, TS-1, and Ti-MCM-41 with a similar Ti loading of 2 wt%, plotted as a function of time-on-stream. Reaction conditions: 5 mmol 2-cyclohexen-1-one, 10 mL acetonitrile, 7.5 mmol H_2O_2 , 0.1 g catalyst, temperature = 343 K.

other nature of the Ti sites in comparison with Ti-Beta. For Ti-MCM-41, the Ti sites are merely located at the external surface of MCM-41,¹⁵ and these Ti sites are less stable and less active than framework Ti sites in the epoxidation with hydrogen peroxide. As shown in Fig. 6, the 2-cyclohexen-1-one conversion over Ti-MCM-41 does not change any more beyond time-on-stream of 2 h, probably due to the quick catalytic deactivation. These results are in good accordance with those reported by Corma *et al.*,¹⁷ who suggested that Ti/ITQ-2 (prepared *via* the same route as Ti-MCM-41) is a suitable catalyst for the epoxidation of olefins only using organic peroxides in the absence of water.

Based on the above-mentioned results, it can be stated that the pore structure of Ti(IV)-containing zeolites do strongly affect their catalytic performances in epoxidation reactions, in great contrast to the results reported by Guidotti *et al.*¹⁸ Furthermore, post-synthesis modified Ti-Beta zeolites containing Ti species, which are mainly incorporated at tetrahedral

framework positions, are robust catalysts for the epoxidation with hydrogen peroxide.

3.3.2. Effects of the Ti loading and the preparation method. The effects of the Ti loading (1–5 wt%) of the Ti-Beta zeolites on the 2-cyclohexen-1-one conversion and product selectivity were further investigated and the results are summarized in Table 2. No 2-cyclohexen-1-one conversion could be observed for Si-Beta as a catalyst, while significant 2-cyclohexen-1-one epoxidation is observed for Ti-Beta with different Ti loadings, indicating that the catalytic activity of Ti-Beta zeolites is exclusively caused by the framework Ti species. Accordingly, the epoxidation activity of Ti-Beta increases with increasing Ti loading. Further analysis suggests that a quasi-linear correlation between the epoxidation rate (in mmol h^{-1}) and the number of tetrahedrally coordinated framework Ti(IV) species (determined by ICP for total Ti number and XPS for T(IV) content) can be drawn (Fig. 7), evidencing that these framework Ti species are responsible for the epoxidation activity. Moreover, the epoxide selectivity (only epoxide and diol can be detected from epoxidation) also increases slightly with increasing Ti loading. This should be due to the existence of remaining silanol nests in the Ti-Beta zeolites with low Ti loadings, and such weakly acidic surface OH groups are capable of catalyzing the hydrolysis of formed epoxides to diol.

The catalytic performances of Ti(IV)-containing Beta zeolites prepared *via* different routes, but with a similar Ti loading of 5 wt% in the epoxidation of 2-cyclohexen-1-one are compared in Table 2. The $\text{TiO}_2/\text{Si-Beta}$ zeolites prepared by wet impregnation (-w) and mechanical mixing (-m) show certain catalytic activity and 2-cyclohexen-1-one conversions of 21.1 and 11.6%, respectively, after a time-on-stream of 5 h. For these materials, selectivities to epoxide of 80.9 and 84.0% were observed. The Ti-H-Beta zeolites appear to be more active than $\text{TiO}_2/\text{Si-Beta}$ and a 2-cyclohexen-1-one conversion of 32.8% can be obtained after a time-on-stream of 5 h. However, the selectivity to

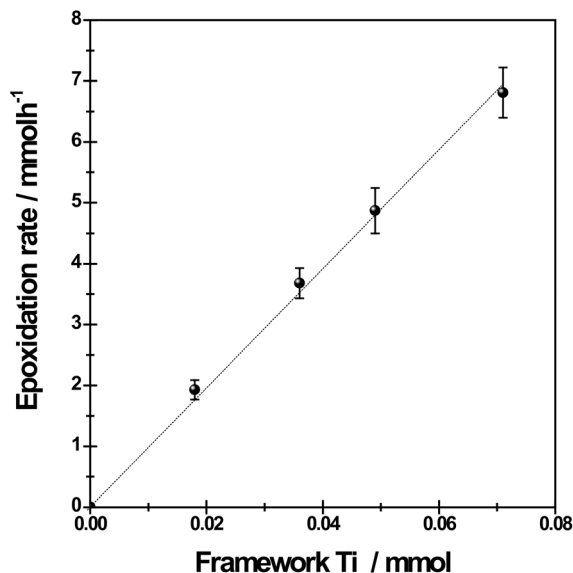


Fig. 7 Correlation between the epoxidation rate and the number of tetrahedrally coordinated framework Ti(IV) species.

epoxide is only 66.2%, and 22.4% diol is obtained caused by the hydrolysis of epoxide, which is catalyzed by residual acid sites. Based on the catalytic activity of Ti(IV)-containing Beta zeolites, it is quite obvious that post-synthesis modified Ti-Beta zeolites are outstanding catalysts for the epoxidation of 2-cyclohexen-1-one in terms of both catalytic activity and epoxide selectivity. It is thus demonstrated that the zeolite host, the organometallic Ti complex and the synthesis procedures are all very important issues to obtain robust Ti(IV)-containing Beta catalysts for epoxidation reactions.

In repeated preparations of 5 wt% Ti-Beta zeolites *via* the two-step post-synthesis procedure, the obtained Ti loadings were quite similar to that in the original experiment. Furthermore, the catalytic performances of the compared materials in the 2-epoxidation, including the 2-cyclohexen-1-one conversion and epoxide selectivity after a time-on-stream of 5 h were almost identical (Table 2, see b). These results strongly indicate that the two-step post-synthesis procedure is a feasible route to obtain Ti-Beta zeolites with excellent reproducibility. We also tested the regeneration ability of Ti-Beta zeolites prepared *via* the post-synthesis route, and a slight decrease in both 2-cyclohexen-1-one conversion and epoxide selectivity occurred. Typically, a 2-cyclohexen-1-one conversion of 50.8% and an epoxide selectivity of 94.1% were obtained after the third use (see c), as shown in Table 2. Since the leaching of Ti species can be excluded according to ICP analysis, the decrease in the epoxidation activity should be due to changes in the nature of the Ti species caused by their interaction with hydrogen peroxide or bulky reaction products as suggested by Carati *et al.*²⁸ and Hutchings *et al.*^{42,43} This is a common problem when using Ti(IV)-containing zeolites as catalysts for the epoxidation with hydrogen peroxide, and a similar decrease in the epoxidation activity can also be observed for commercial TS-1 (Fig. S5†).

Table 2 Catalytic properties of the Ti-Beta zeolites under study in the epoxidation of 2-cyclohexen-1-one^a


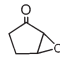
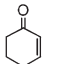
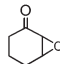
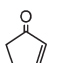
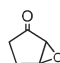
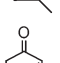
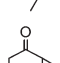
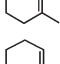
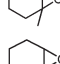
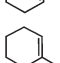
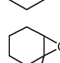
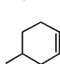
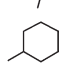
Sample	Ti loading (wt%)	Conv. (%)	Selectivity (%)		
			Epoxide	Diol	Others
Si-Beta	0	0	/	/	/
1 wt% Ti-Beta	1.0	48.6	92.9	4.7	2.4
2 wt% Ti-Beta	1.9	61.6	94.8	3.9	1.3
3 wt% Ti-Beta	2.8	70.2	96.0	3.5	0.5
5 wt% Ti-Beta	4.1	75.3	98.9	1.1	0
5 wt% Ti-Beta ^b	4.1	75.5	98.7	1.3	0
5 wt% Ti-Beta ^b	4.2	74.9	99.0	1.0	0
5 wt% Ti-Beta ^c	4.0	50.8	94.1	1.7	4.2
$\text{TiO}_2/\text{Si-Beta-w}^d$	4.7	21.1	80.9	5.1	14.0
$\text{TiO}_2/\text{Si-Beta-m}^e$	4.9	11.6	84.0	6.1	9.9
Ti-H-Beta ^f	4.6	32.8	66.2	22.4	11.4

^a Reaction conditions: 5 mmol 2-cyclohexen-1-one, 10 mL MeCN, 7.5 mmol H_2O_2 , 0.1 g catalyst, temperature = 343 K, time-on-stream = 5 h. ^b Repeated experiments. ^c Third use. ^d Prepared by wet impregnation of Si-Beta with TBOT. ^e Prepared by mechanical mixing of Si-Beta with TiO_2 (Degussa P25). ^f Prepared by grinding H-Beta with Cp_2TiCl_2 .

3.3.3. Effects of solvents on the epoxidation activity of Ti-Beta. It is well known that solvents may show a vital effect on the catalytic performances of Ti(IV)-containing zeolites in liquid phase oxidation reactions.^{20,44,45} Such a unique effect is generally acknowledged as referring to two different active species I and II, as shown in Fig. S6.† For species I, a stable five-ring structure is formed by the coordination of ROH to a Ti site and hydrogen bondings to the Ti-peroxy complex, which are believed to be the active intermediates in protic alcohol solvents. In the case of aprotic solvents, species II is assumed to contribute to the active substrates. In addition, the polarity expressed in terms of the dielectric constant, geometry of the solvent and its interaction with the active centers are also of significant importance. Table 3 summarizes the influence of solvents on the catalytic performance of the 5 wt% Ti-Beta zeolite for the epoxidation of 2-cyclohexen-1-one with hydrogen peroxide. Typically, protic solvents, *e.g.* MeOH, EtOH, and *t*-BuOH, and aprotic solvents, *e.g.* MeCN, MeCOMe, and MeCOEt, are selected as solvents. It is clearly seen that the epoxidation activity increases with increasing solvent polarity in the case of using both protic and aprotic solvents. However, the epoxide selectivity decreases with increasing solvent polarity in the case of using protic solvents, while it increases with increasing polarity using aprotic solvents. Among protic alcohol solvents, in contrast to MeOH and EtOH, *t*-BuOH leads to distinct lower activity, which could be attributed to a decrease in the electrophilicity of species I and to serious steric constraints on its formation.⁴⁶ Whereas, using MeOH and EtOH as solvents results in a significant decline in the 2-cyclohexen-1-one epoxide selectivity due to solvolysis effects, which leads to a sharp increase in the formation of glycol monomethyl ether or monoethyl ether, as shown in Table 3. As a whole, aprotic MeCN seems to be the best choice of solvent in view of substrate conversion and epoxide selectivity. The favorable effects of MeCN are, on the one hand, associated with its weak basic nature, which can effectively neutralize the weak acid sites generated in Ti-Beta, and therefore, suppress the hydrolysis of epoxide products.⁴⁷ On the other hand, MeCN molecules can be activated by the electrophilicity of Ti species to react with hydrogen peroxide to form the peroxyimide intermediate, CH₃-C(=NH)-O-O-H, which is known to be an active oxidizing agent toward organic substrates.⁴⁸

3.3.4. Effects of the substrate on the epoxidation performances. Table 4 shows the catalytic results of the 5 wt% Ti-Beta zeolite in the epoxidation of various unsaturated organic compounds. It is seen that the epoxidation of unsaturated five-ring ketones is relatively slower than the epoxidation of six-ring ketones, in accord with the earlier results of Tatsumi *et al.*^{20,22} This should be ascribed to the resonance interaction between the C=C double bond and the electron-withdrawing C=O groups. The coplanar atoms of the C=C-C=O system result in an electron deficiency at the C=C double bond of 2-cyclopenten-1-one and its derivatives, which subsequently reduces the reactivity. In the case of 2-cyclohexen-1-one, the preferential conformation excludes the existence of a coplanar C=C-C=O system, and therefore, the conjugative effect does not exist. Actually, the C=C double bond in 2-cyclohexen-1-one is similar to an isolated C=C double bond and high epoxidation

Table 4 Epoxidation of various unsaturated compounds over the 5 wt % Ti-Beta/H₂O₂ system

Substrate	Product	Conv. (%)	Selectivity (%)		
			Epoxide	Diol	Others
		43.8 ^a	>99.9	0	0
		75.3 ^a	98.9	1.1	0
		<0.1 ^a	/	/	/
		5.8 ^a	64.7	18.3	17.0
		46.8 ^b	58.3	14.9	26.8
		48.8 ^b	23.6	28.9	47.5
		28.9 ^b	46.5	19.6	33.9

^a Reaction conditions: 5 mmol substrate, 10 mL MeCN, 7.5 mmol H₂O₂, 0.1 g catalyst, temperature = 343 K, time-on-stream = 5 h.

^b Temperature = 333 K, time-on-stream = 2 h.

Table 3 Effect of solvents on the epoxidation of 2-cyclohexen-1-one over the 5 wt% Ti-Beta/H₂O₂ system^a

Solvent	Polarity	Dielectric constant	Conv. (%)	Selectivity (%)			
				Epo.	Diol	Glycol ether	Others
Methanol	Protic	32.7	85.7	45.1	3.3	38.4	13.2
EtOH	Protic	24.5	82.6	48.7	2.8	36.7	11.8
<i>t</i> -BuOH	Protic	10.9	60.7	90.2	2.1	2.5	5.2
MeCN	Aprotic	37.5	75.3	98.9	1.1	0	0
MeCOMe	Aprotic	20.7	53.7	84.6	15.4	0	0
MeCOEt	Aprotic	18.5	51.8	81.7	18.3	0	0

^a Reaction conditions: 5 mmol 2-cyclohexen-1-one, 10 mL solvent, 7.5 mmol H₂O₂, 0.1 g catalyst, temperature = 343 K, time-on-stream = 5 h.

activity can be achieved using the 5 wt% Ti-Beta zeolite as a catalyst. In addition, the dramatic decline in the conversion of methyl substituted substrates, such as 3-methyl-2-cyclopenten-1-one and 3-methylcyclohexen-1-one, implies that steric constraints on the substrate should be seriously considered. As a whole, it can be concluded that both the electron deficiency and steric effect play important roles in the epoxidation of α,β -unsaturated ketones over Ti-Beta/H₂O₂ system.

Meanwhile, the rate of solvolysis, which transforms epoxide into the corresponding diol, is dependent on the structure of the epoxide formed. Hence, the effect of substituting methyl groups on the corresponding epoxide selectivity is worth investigating. In order to eliminate the electron deficiency and steric effect, 1-methyl and 4-methyl substituted cyclohexenes are selected as model substrates and the results are shown in Table 4. Compared with 4-methylcyclohexene having a methyl group located at the position far from the double bond, the hydrolysis rate is relatively higher in the case of a methyl group located on the olefinic double bond, *i.e.* 1-methylcyclohexene. The higher hydrolysis rate will result in a low epoxide selectivity, which can be ascribed to the facile ring-opening generating a tertiary carbenium cation followed by the nucleophilic attack on the cation *via* the SN₁ mechanism.⁴⁸

4. Conclusion

In the present study, a reproducible and scalable two-step post-synthesis procedure has been developed to prepare Ti(IV)-containing Beta zeolites. In the first step, commercial H-Beta zeolites are dealuminated to Si-Beta by treating in concentrated nitric acid solution and vacant T sites with associated silanol groups are created. In the second step, the organometallic Ti complex Cp₂TiCl₂ interacts with vacant T sites in the Si-Beta zeolite and Ti species are subsequently incorporated into the framework of Beta zeolite upon calcination. This preparation procedure and the corresponding mechanism are described according to the characterization results from DRIFT and multinuclear solid-state NMR spectroscopy (¹H MAS NMR, ²⁷Al MAS NMR, and ²⁹Si MAS NMR). Dominating tetrahedrally coordinated Ti(IV) species in the zeolite framework, together with a minority of octahedrally coordinated Ti(VI) species at framework or extra-framework positions, could be clearly identified by means of UV-vis spectroscopy and XPS. The above-mentioned post-synthesis procedure can be simply extended to the preparation of other metal ions incorporated into zeolite frameworks providing that the dealumination of the zeolite host is possible and a suitable organometallic complex is available.

The Ti-Beta zeolites were successfully applied as catalysts in the epoxidation of unsaturated ketones, *e.g.* 2-cyclohexen-1-one, with hydrogen peroxide as an oxidant. High epoxidation activity as well as high selectivity toward epoxide were simultaneously obtained over Ti-Beta, far better than TS-1 and Ti-MCM-41 reference materials.

Furthermore, the impacts of the preparation methods and Ti loadings on the catalytic performances of Ti-Beta zeolites were investigated. The two-step post-synthesis method appears to be the most feasible route to prepare robust Ti-Beta catalysts for the epoxidation of 2-cyclohexen-1-one with hydrogen peroxide. A quasilinear correlation between the epoxidation rate and the number of tetrahedrally coordinated framework Ti species could be drawn for Ti-Beta zeolites, evidencing that these Ti species are responsible for the epoxidation activity. For the epoxidation with hydrogen peroxide, the solvent has a great impact on the catalytic performance of the Ti-Beta zeolites, and aprotic MeCN appears to be the best choice of solvent in view of substrate conversion and epoxide selectivity. When different unsaturated organic compounds are employed for the epoxidation with hydrogen peroxide, the electron deficiency, steric effects, and substituted groups of the substrate may influence the catalytic performances of Ti-Beta zeolites.

Acknowledgements

This work was financially supported by the National Natural Science Foundation of China (21373119) and the Ministry of Education of China (NCET-11-0251, IRT13022). The support from 111 Project (B12015) and the Collaborative Innovation Center of Chemical Science and Engineering (Tianjin) is also acknowledged. Furthermore, M.H. wants to acknowledge financial support by Deutsche Forschungsgemeinschaft.

References

- 1 M. Taramasso, G. Perego and B. Notari, *U.S. Patent*, no. 4,410,501, 1983.
- 2 D. R. C. Huybrechts, L. De Bruycker and P. A. Jacobs, *Nature*, 1990, **345**, 240.
- 3 F. Cavanj and J. H. Teles, *ChemSusChem*, 2009, **2**, 508.
- 4 A. Corma, M. A. Camblor, P. Esteve, A. Martínez and J. Pérez-Pariente, *J. Catal.*, 1994, **145**, 151.
- 5 A. Corma, P. Esteve, A. Martínez and S. Valencia, *J. Catal.*, 1995, **152**, 18.
- 6 T. Tatsumi and N. Jappar, *J. Phys. Chem.*, 1998, **102**, 7126.
- 7 P. Wu, T. Tatsumi, T. Komatsu and T. Yashima, *J. Phys. Chem. B*, 2001, **105**, 2897.
- 8 P. Wu, Y. Liu, M. He and T. Tatsumi, *J. Catal.*, 2004, **228**, 183.
- 9 M. A. Camblor, A. Corma, A. Martínez and J. Pérez-Pariente, *J. Chem. Soc., Chem. Commun.*, 1992, 589.
- 10 T. De Baerdemaeker, B. Steenackers and D. De Vos, *Chem. Commun.*, 2013, **49**, 7474.
- 11 N. Jappar, Q. H. Xia and T. Tatsumi, *J. Catal.*, 1998, **180**, 132.
- 12 T. Blasco, M. A. Camblor, A. Corma, P. Esteve, A. Martínez, C. Prieto and S. Valencia, *Chem. Commun.*, 1996, 2367.

- 13 J. Lu, K. M. Kosuda, R. P. Van Duyne and P. C. Stair, *J. Phys. Chem. C*, 2009, **113**, 12412.
- 14 J. P. Nogier, Y. Millot, P. P. Man, T. Shishido, M. Che and S. Dzwigaj, *J. Phys. Chem. C*, 2009, **113**, 4885.
- 15 T. Maschmeyer, F. Rey, G. Sankar and J. M. Thomas, *Nature*, 1995, **378**, 159.
- 16 R. D. Oldroyd, J. M. Thomas, T. Maschmeyer, P. A. MacFaul, D. W. Snelgrove, K. U. Ingold and D. D. M. Wayner, *Angew. Chem., Int. Ed. Engl.*, 1996, **35**, 2787.
- 17 A. Corma, U. Díaz, V. Fornés, J. L. Jordá, M. Domine and F. Rey, *Chem. Commun.*, 1999, 779.
- 18 M. Guidotti, N. Ravasio, R. Psaro, G. Ferraris and G. Moretti, *J. Catal.*, 2003, **214**, 242.
- 19 T. Punniyamurthy, S. Velusamy and J. Iqbal, *Chem. Rev.*, 2005, **105**, 2329.
- 20 M. Sasidhara, P. Wu and T. Tatsumi, *J. Catal.*, 2002, **205**, 332.
- 21 G. Fioroni, F. Fringuelli, F. Pizzo and L. Vaccaro, *Green Chem.*, 2003, **5**, 425.
- 22 X. H. Shen, W. B. Fan, Y. He, P. Wu, J. G. Wang and T. Tatsumi, *Appl. Catal., A*, 2011, **401**, 37.
- 23 M. G. Clerici and U. Romano, *US Patent* 4,937,216, 1990.
- 24 K. A. Kayano and T. Tatsumi, *Chem. Commun.*, 1996, 145.
- 25 M. R. Boccuti, K. M. Rao, A. Zecchina, G. Leofanti and G. Petrini, *Stud. Surf. Sci. Catal.*, 1989, **48**, 133.
- 26 M. Sasidharan and A. Bhaumik, *Phys. Chem. Chem. Phys.*, 2011, **13**, 16282.
- 27 L. Marchese, T. Maschmeyer, E. Gianotti, S. Coluccia and J. M. Thomas, *J. Phys. Chem. B*, 1997, **101**, 8836.
- 28 A. Carati, C. Flego, E. P. Massara, R. Millini, L. Carluccio, W. O. Parker Jr. and G. Bellussi, *Microporous Mesoporous Mater.*, 1999, **30**, 137.
- 29 J. P. Nogier, Y. Millot, P. P. Man, C. Méthivier, M. Che and S. Dzwigaj, *Catal. Lett.*, 2009, **130**, 588.
- 30 P. Fejesa, J. B. Nagy, J. Halász and A. Oszkó, *Appl. Catal., A*, 1998, **175**, 89.
- 31 C. D. Wagner, W. M. Riggs, L. E. Davis, J. F. Moulder and G. E. Muilenberg, *Handbook of X-ray photoelectron spectroscopy: a reference book of standard data for use in x-ray photoelectron spectroscopy*, Perkin-Elmer, MN, Eden-Prairie, 1979.
- 32 L. Li and N. Guan, *Microporous Mesoporous Mater.*, 2009, **117**, 450.
- 33 S. Dzwigaj, J. Janas, J. Gurgul, R. P. Socha, T. Shishido and M. Che, *Appl. Catal., B*, 2009, **85**, 131.
- 34 J. Janas, T. Machej, J. Gurgul, R. P. Socha, M. Che and S. Dzwigaj, *Appl. Catal., B*, 2007, **75**, 239.
- 35 S. Dzwigaj and T. Shishido, *J. Phys. Chem. C*, 2008, **112**, 5803.
- 36 X. Wang, W. Dai, G. Wu, L. Li, N. Guan and M. Hunger, *Microporous Mesoporous Mater.*, 2012, **151**, 99.
- 37 M. Hunger, S. Ernst and J. Weitkamp, *Zeolites*, 1995, **15**, 188.
- 38 P. Li, G. Q. Liu, H. H. Wu, Y. M. Liu, J. G. Jiang and P. Wu, *J. Phys. Chem. C*, 2011, **115**, 3663.
- 39 M. Hunger, S. Ernst, S. Steuernagel and J. Weitkamp, *Microporous Mater.*, 1996, **6**, 349.
- 40 M. Hunger, *Catal. Rev. Sci. Eng.*, 1997, **39**, 345.
- 41 Y. Jiang, J. Huang, W. Dai and M. Hunger, *Solid State Nucl. Magn. Reson.*, 2011, **39**, 116.
- 42 L. J. Davis, P. McMorn, D. Bethell, P. C. Bulman Page, F. King, F. E. Hancock and G. J. Hutchings, *J. Catal.*, 2001, **198**, 319.
- 43 L. J. Davis, P. McMorn, D. Bethell, P. C. Bulman Page, F. King, F. E. Hancock and G. J. Hutchings, *J. Mol. Catal. A: Chem.*, 2001, **165**, 243.
- 44 W. B. Fan, P. Wu, S. Namba and T. Tatsumi, *J. Catal.*, 2006, **243**, 183.
- 45 W. B. Fan, P. Wu and T. Tatsumi, *J. Catal.*, 2008, **256**, 62.
- 46 M. G. Clerici and P. Ingallina, *J. Catal.*, 1993, **140**, 71.
- 47 A. Corma, P. Esteve and A. Martinez, *J. Catal.*, 1996, **161**, 11.
- 48 G. Grigoropoulou, J. H. Clark and J. A. Elings, *Green Chem.*, 2003, **5**, 1.